Research Article

Temperature fluctuations and ventilation dynamics induced by atmospheric pressure variations in Lamalunga Cave (Apulia, Italy) and their influences on speleothem growth

Andrea Borsato[a] (iD), Marco Samadelli[b], Vincenzo Martimucci[c] and Giorgio Manzi[d]

[a]School of Environmental and Life Sciences, The University of Newcastle, Australia; [b]EURAC Research, Institute for Mummy Studies, Bolzano, Italy; [c]C.A.R.S. - Centro Altamurano Ricerche Speleologiche, Italy and [d]Department of Environmental Biology, Sapienza University of Rome, Rome, Italy

Abstract

Lamalunga Cave (Altamura, Southern Italy) is renowned for the discovery in 1993 of an excellently preserved Neanderthal skeleton. Given the importance of the findings and the potential use of Lamalunga speleothems for paleoclimate reconstructions, a detailed monitoring program was undertaken to investigate the connections between microclimate parameters and speleothem growth. The cave air temperature is characterized by annual sinusoidal cycles with increasing phase shift and decreasing thermal amplitude from $\pm 2.1°C$ to $\pm 0.04°C$ as a function of increasing rock overburden, and daily to sub-daily cycles induced by surface air pressure (SAP) variations characterized by strong 24-hour and 12-hour solar harmonic frequencies, with thermal amplitude decreasing from $0.0054°C$ to $0.0021°C$ in the deeper parts of the cave. The ventilation regime is mainly controlled by SAP fluctuations. Fast SAP rises can trigger "emptying events" during which most of the cave air is replaced and the CO_2 concentration falls towards near-atmospheric values. The steady and gentle ventilation created by SAP fluctuations also influences the growth and morphology of calcite coralloids, with larger popcorn assemblages concentrated in the northern galleries and delicate branching morphologies prevailing along the South Gallery where stable temperature and relative humidity conditions occur. The study is a seminal example of how high-precision measurements of cave air temperature can provide a wealth of information on cave ventilation and thermal regime and provide valuable support for robust paleoclimate reconstruction from speleothems.

Keywords: Lamalunga, Cave microclimate, Cave ventilation, Thermal diffusivity, Pressure-induced temperature variations, Barometric tides, Calcite coralloids, Speleothems

(Received 28 February 2023; accepted 14 November 2023)

INTRODUCTION

Cave ventilation and air temperature fluctuations play crucial roles in controlling speleothem growth rate, as well as influencing their morphology and internal fabrics (Spötl et al., 2005; Treble et al., 2015; Mattey et al., 2016). When coupled with dripwater hydrochemistry, they can unravel the seasonality of speleothem growth and, therefore, microclimate studies, which are the backbone of any correct paleoclimate reconstruction from speleothems (Mattey et al., 2010; Tremaine and Froelich, 2013; Warken et al., 2018; Riechelmann et al., 2019). Cave ventilation studies imply long-term monitoring of cave-air CO_2, temperature, relative humidity, and, ideally, 222-Radon (Breitenbach et al., 2015; Mattey et al., 2016; Prelovšek et al., 2018; Kukuljan et al., 2021; Sekhon et al., 2021; Sainz et al., 2022). However, recent studies demonstrated that a wealth of information also can be derived by statistical analyses of surface air

pressure and high-resolution (0.001°C) temperature time-series at different depths within the cave (Perrier et al., 2023).

We used this approach coupled with seasonal measurements of other relevant microclimate variables in Grotta di Lamalunga, a cave renowned for the discovery in 1993 of a Neanderthal skeleton in an excellent state of preservation (Pesce Delfino and Vacca, 1993; Lari et al., 2015). The skeleton, which represents a unique example of an almost complete non-modern human, lies the end of a small chamber called Abside dell'Uomo (Apse of Man) (Fig. 1), is partially embedded in a calcite coating, and encrusted by myriad calcite coralloids (Vanghi et al., 2017, 2019) (Fig. 2).

Given the exceptional importance of the finding, permit was given to remove only fragments of the right scapula, whose paleogenetic mitochondrial DNA revealed that the bone belonged to a typical Neanderthal morphotype (Lari et al., 2015). U–Th dating of the calcite crust immediately coating the bone yielded an age between 130.1 ± 1.9 ka and 172 ± 15 ka (Lari et al., 2015). These exceptional data resulted in new research activities financed by the Italian Ministry of Instruction, University and Research (MIUR), including morphological study of the scapula (Di Vincenzo et al., 2019), in-situ observations on the dentition and
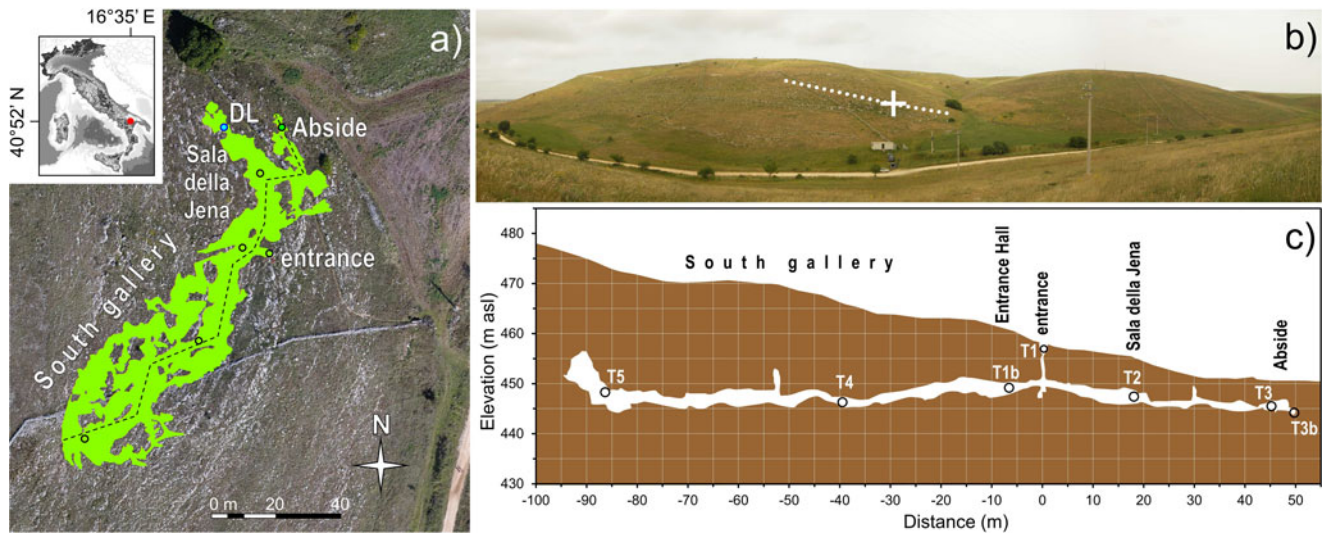
Figure 1. (a) Location map (Italy insert) and plan view of Lamalunga Cave near Altamura (simplified from Centro Altamurano Ricerche Speleologiche map); the dashed line represents the position of the cross section in (b, c), black circles indicate the positions of the temperature loggers, blue circle indicates the position of the drip logger (DL) in the Northern End. (b) Panoramic view from SE of Lamalunga valley with the location of the cave entrance (white cross) and the surface intersection of the central axis of the cave (dotted line). (c) Simplified cross section of the Lamalunga Cave with the position of the temperature loggers. The horizontal distances are calculated from the cave entrance.

oral cavity (Riga et al., 2020), and virtual reconstruction and external morphological analysis of a 3D model of the cranium (Profico et al., 2023). Concurrently, a detailed monitoring program was carried out to assess the current conditions for preservation of the skeleton. In this work we present the results of three years of temperature and microclimate monitoring, while a companion paper will discuss the cave hydrochemical and microbiological conditions, as well as the conservation state of the archaeological remains.

Lamalunga Cave description

Lamalunga Cave (40°52′18″N, 16°35′15″E, entrance elevation 454 m asl) is located on the High Murge karstic plateau (Parise, 2011) close to the town of Altamura in Apulia, southern Italy, 35 km from the Adriatic Sea. It consists in a single horizontal gallery 125 m long, and 15–25 m wide, with several interconnected lateral branches for a total mapped length of 1247 m, a maximum depth of 24 m and an estimated total volume of about 6000 m^3 (Fig. 1). The cave is cut within the well-bedded, shallow-marine Upper Cretaceous Calcare di Altamura limestone (Zezza, 2000), which developed during the Pliocene and Pleistocene in the uppermost vadose level of the karstic system and now is capped by barren karst morphology with scarce and patchy soil cover and (Agostini, 2011). The High Murge landscape is characterized by remnants of fluvio-karst and large karst features (valleys,
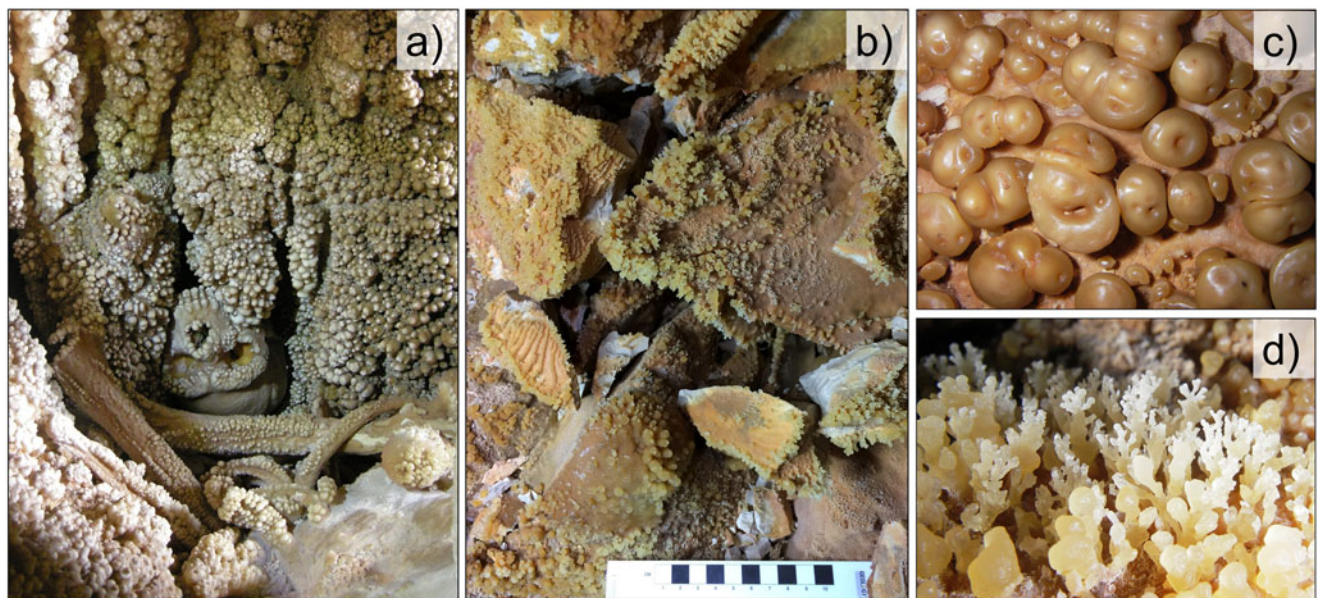

Figure 2. Morphology of coralloid formations. (a) The Neanderthal bones in the Abside chamber coated by popcorn calcite coralloids. The Neanderthal cranium in the center of the picture is upside-down and provides a generalized scale (credit: Soprintendenza A.B.A.P. per la C.M. di Bari, Puglia). (b) Branching calcite coralloids growing on limestone debris on the floor of South Gallery. (c) Details of popcorn coralloids (base of picture = ∼50 mm); (d) Details of branching coralloids (base of picture = ∼50 mm).

dolines, and complex depressions) and is punctuated by a network of explored caves that developed up to a few hundreds of meters below the surface (Parise, 2011). The only access to Lamalunga Cave is a 7-m deep shaft about 1 m in diameter that opens on the SE-facing slope of a karst valley and intersects the main gallery on its East flank. The 0.5×0.5 m key-hole passage between the bottom of the entrance shaft and the main gallery was artificially enlarged in 1993 by members of the local speleological society, Centro Altamurano Ricerche Speleologiche (C.A.R.S.). Following discovery of the faunal and human remains, access to the cave was closed by a double trapdoor at the surface, while the natural ventilation of the cave was secured by a series of narrow fissures at the base of the trapdoor. At present, the trapdoor is open only during the occasional visits to the cave ($\sim$1–4 visits per year) and remains open for the entire period in which the visitors are inside the cave (ca. 2–8 hours per visit). Apart for these short periods, the double trapdoor remains closed, and ventilation occurs through the few narrow fissures at its base.

The southern part of the cave (South Gallery) is characterized by the occurrence of fossil speleothems, which commonly are broken or corroded, and widespread angular debris that originated from collapses and rock detachments from the wall and ceiling. Active speleothem formation occurs almost exclusively in the northern part of the cave and consists in a few small stalagmites, thin flowstones, and coatings. The northern galleries of the cave (Sala Jena, Abside dell'Uomo) also are characterized by extensive popcorn coralloid formations, particularly in the gallery leading to Abside dell'Uomo (Fig. 2a), where most of the active dripping is concentrated (Vanghi et al., 2017, 2019). Along the South Gallery, calcite coralloids are less common than in the northern galleries and show more minute and delicate morphologies (Fig. 2b). Coralloids, which mark the last phase of cave calcite deposition, coat limestone debris, speleothems, and fossil animal bones scattered along the cave floor (Zezza, 2000; Agostini, 2011). Uranium-series dating revealed that most of the coralloid growth occurred between 64 and 36 ka and in the Holocene with growth rates oscillating between 0.2 mm/ka and 0.5 mm/ka (Vanghi et al., 2019); these two growth phases are separated by several hiatuses with corroded surfaces that correspond to the time interval of the cold Marine Oxygen Isotope Stage 2 (Lisiecki and Raymo, 2005) and the local last glacial maximum between ca. 30 and 14 ka BP (Follieri et al., 1998).

Cave microclimate physics

Inner sections of caves with a single entrance commonly have a stable temperature during the year, which usually corresponds to the surface mean annual temperature (Jeannin et al., 1997; Badino, 2010). The geothermal flux from the saturated zone is usually counteracted by infiltrating water and cave ventilation, which ensure low vertical thermal gradient in most karstic areas (Luetscher and Jeannin, 2004; Badino, 2010). At the same time, the relative humidity in sections away from the entrance is at near saturation (99–100%) for most of the year, with the exception of highly ventilated and near-entrance galleries (Badino, 2010; Bourges et al., 2014).

Ventilation, the exchange of cave air with the surface atmosphere, directly affects temperature, humidity, and cave air CO_2 dynamics (Luetscher and Jeannin, 2004; Badino, 2010; Gregorič et al., 2014). Cave ventilation is driven by diurnal and seasonal variations in air density between surface and cave air. These density variations can result from differential warming at the surface

and in the caves, as well as from atmospheric pressure variations and water-flow conditions (Bourges et al., 2014; Vieten et al., 2016). Caves with multiple entrances are characterized by convective airflow circulation (chimney effect), resulting in large seasonal and daily fluctuations in relative humidity and temperature, and CO_2 concentrations similar to surface values (Faimon et al., 2012). In summer, the cold cave air escapes by the lower opening and draws in warm outside air, while in winter the warm cave air escapes from the upper opening and drags cold outside air through the lower opening.

The effectiveness of ventilation also depends on the confinement state of each gallery inside the cave. Caves with a single opening that is almost barred by a scree, or remote dead-end galleries, are the most confined situations. There, relative humidity is near saturation, seasonal changes in temperature are almost completely buffered by rock thermal inertia, temperature changes are only due to the heat generated during compression or expansion of air induced by pressure changes (Bourges et al., 2014), and CO_2 concentration values are significantly higher than at the surface (Ek and Gewelt, 1985; Faimon and Ličbinská, 2010; Bourges et al., 2014; Borsato et al., 2015). In these caves, the exchange between surface and cave air is determined by the area of the entrance with respect to the entire volume of the underground passages.

A particular case of single-entrance caves is barometric caves, which are characterized by a narrow entrance and large underground volume (Badino, 2010; Gomell and Pflitsch, 2022). In these caves, the atmospheric pressure variations are not transmitted instantaneously to the deeper parts of the cave and the galleries are crossed by barometric airflow circulation or "reversing air currents" (Wigley and Brown, 1969). In temperate climate settings characterized by important seasonal temperature excursions, the thermal amplitude in cave passages (i.e., the seasonal temperature excursion) is mainly controlled by the thickness of rock and soil cover and their thermal diffusivity (Badino, 2010; Domínguez-Villar et al., 2013, 2023; Guerrier et al., 2019).

Cave air CO_2 concentration directly affects dripwater degassing and its pH and, thus, calcite supersaturation. Given that the CO_2 concentrations in soil are orders of magnitude greater than atmospheric values, percolating water is usually enriched in CO_2 with respect to the cave atmosphere (Ek and Gewelt, 1985; Spötl et al., 2005; Frisia et al., 2011; Breecker et al., 2012; Mattey et al., 2016) and tend to lose CO_2 (degassing) when entering the cave, thus shifting the pH towards more alkaline values and raising the water supersaturation for calcium carbonate minerals. The greater the difference between infiltration water and cave atmosphere pCO_2, the higher will be the rise in supersaturation and, thus, the speleothem growth rate (Borsato et al., 2015).

MATERIALS AND METHODS

Two meteorological stations in proximity of the cave were utilized for comparison of the Lamalunga Cave data: Altamura station (40°49′N, 16°34′E; elevation 458 m asl) located 6 km SW from the cave, and Quasano station (40°58′N, 16°35′E; elevation 369 m asl) located 10 km N from the cave entrance. Meteorological data (daily min and max temperatures, daily rainfall amount, air pressure) were downloaded from the monitoring network of Protezione Civile Puglia (https://protezionecivile. puglia.it/rete-di-monitoraggio-e-dati-meteo-idrometrici).

Cave temperatures were measured at 1-hour intervals with seven calibrated and certified TinyTag TGP-4017 and TGP-4500

data loggers characterized by an accuracy better than 0.5°C and a resolution (incremental readings) of 0.00144°C (temperature range +70°/−25°C, 16-bit resolution). The reproducibility of the temperature readings was also tested inside the cave by leaving the loggers for 24 hours in the farther end of the cave, which was characterized by daily thermal variation less than 0.02°C, resulting in discrepancies between the different loggers of less than 0.08°C. The internal noise of the temperature loggers was also tested by measuring the mean absolute value of the difference between the hourly temperature readings and their 24-hour running means. The average value of three different dataloggers tested for six continuous days in the absence of meteorological perturbation (5–10 August 2019) resulted in a natural noise of 0.0011 ± 0.0002°C, a value similar to the incremental resolution of the loggers.

Thermal daily residuals, as well as surface air-pressure residuals, were calculated as differences between the hourly values and their 24-hour centered running means. Pool-water temperature was measured using a WTW TetraCon 325 dual probe (resolution ± 0.01°C, accuracy ± 0.2°C), while dripwater temperature was measured with a Horiba LAQUAtwin EC 22 Conductivity Meter (resolution ± 0.1°C, accuracy ± 0.3°C). Both temperature probes were equilibrated and tested in a large water pool in the cave against the TinyTag TGP-4500 loggers.

Relative humidity was measured hourly by using TinyTag TGP-4500 data loggers (resolution 0.1% RH, accuracy ± 2.0% RH, not saturated). Spot measurements during different visits to the cave also were made with a Vaisala HM70 hand-held humidity and temperature meter with HMP75B preheated probe with accuracy better than ± 1% RH in the range 0–30°C. Cave air CO_2 concentration was measured with a Vaisala MI70 Measurement Indicator and CARBOCAP GMP222 probe, with measurement accuracy of ± 3.5%. Drip rate was measured every 30 min with Stalagmate automatic drip logger and checked regularly with a chronometer during each visit to the cave.

The air flow in the key-hole passage was estimated by repeated measurements of the velocity of smoke puffs using a stopwatch. The rock cover above each point in Lamalunga Cave was calculated from the laser-scan map of the cave coupled with drone mapping of the surface above, with an estimated error of less than ± 0.2 m.

RESULTS AND DISCUSSION

Surface and cave climatology: annual cycles and thermal diffusivity

The mean annual precipitation recorded at Altamura in the last 20 years was 622 ± 98 mm. Rainfall is concentrated in the autumn and winter months (mean precipitation 63 mm/month), while the summer months (JJA) are the driest (32 mm/month). Mean annual temperature (MAT) at Altamura for the last 60 years (mean 14.85 ± 0.87°C) showed a steady increase of more than 2°C from 1980 to 2015, while a decreasing trend was observed from 2015 to 2020 (Fig. 3). High temperatures coupled with low precipitation during the warm season result in a negative budget between rainfall and potential evapotranspiration with almost no infiltration May–September, while most of the total infiltration (94% of the total 250 mm/yr) occurs during the late autumn and early spring, from November to March (Fig. 3). The hydrology of Lamalunga Cave reflects the surface observations: a stalactite drip rate monitored in the northern end of the cave between 2017 and 2020 revealed that active infiltration starts in early November and

typically lasts until May. In winter and spring, the infiltration is triggered by rainfall events >15–20 mm, while during the dry season the rainfall events triggering infiltration peaks in the stalactite record usually exceed 40 mm.

The surface MAT during the period 2017–2020 (mean: 15.53 ± 7.70°C) follows nearly sinusoidal cycles with maximum values around 24 July and minimal values around 23 January each year, with a thermal amplitude $Ta = \pm 4.95$°C (Fig. 4). The temperature cycles of the 3-year dataset were modeled with the sinusoidal function:

$$T_x = \text{MAT} + A_z \bullet \sin\left(\frac{2\pi t}{365.242}\right) - \varphi_z + \varepsilon \qquad (1)$$

where Tx is the temperature at any time t (in days), MAT is the mean annual temperature, A_z is the amplitude of the annual temperature excursion, 365.242 is the period representing the duration in days of the tropical year, φ_z is the is the phase shift and ε is the initial phase shift of the cycle expressed in radians. The optimal parameters of the three variables MAT, A_z, and φ_z were calculated interactively with the least-squares method by minimizing the sum of squared residuals between the modeled and the measured temperatures during the 3-year observational period.

The temperature measurements in the five locations inside the cave exhibit a much clearer sinusoidal cyclicity, with different mean annual values, phase shift, and thermal attenuation with respect to the external temperature signal (Fig. 4). By using the same approach as for the external temperature, we modeled the sinusoidal temperature cycles by fitting the time-series with the least-squares method.

$$T_x = T_z + A_z \bullet \sin\left(\frac{2\pi t}{365.242}\right) - \varphi_z + \varepsilon \qquad (2)$$

Where Tx is the temperature at any time t (in days), Tz is the mean annual temperature at depth z, and A_z is the amplitude of the annual temperature excursion. The calculated parameters document a decrease in the thermal amplitude A_z and increase in the phase shift (ε) as a function of increasing rock cover above the ceiling of the cave (Table 2).

Near-sinusoidal annual cycles in cave air temperature have been documented in several studies, and are particularly clear in shallow caves (Buecher, 1999; Mattey et al., 2010; Domínguez-Villar et al., 2013, 2023; Breitenbach et al., 2015; Guerrier et al., 2019; Sainz et al., 2022; Perrier et al., 2023). Domínguez-Villar et al. (2013) studied the attenuation of the annual thermal amplitude in a shallow barometric cave in central Spain and highlighted an inverse-linear relationship between the thickness of rock/soil and the natural logarithm of the thermal amplitude at each site (Fig. 5b). Similarly, heat transmission in conduction-dominated soil and rock profiles exhibits a linear correlation between the phase shift and rock/soil thickness related to the exponential amplitude attenuation with depth (Smerdon et al., 2003; Fig. 5a). In fact, the propagation of a temperature signal as a function of time (t) and depth (z) is described by the function:

$$T(z, t) = T_a e^{-kz} \cos\left(\omega t + \varepsilon - kz\right) \qquad (3)$$

where T_a and ω are the amplitude and angular frequency of the harmonic surface temperature, respectively, k is the wave vector,
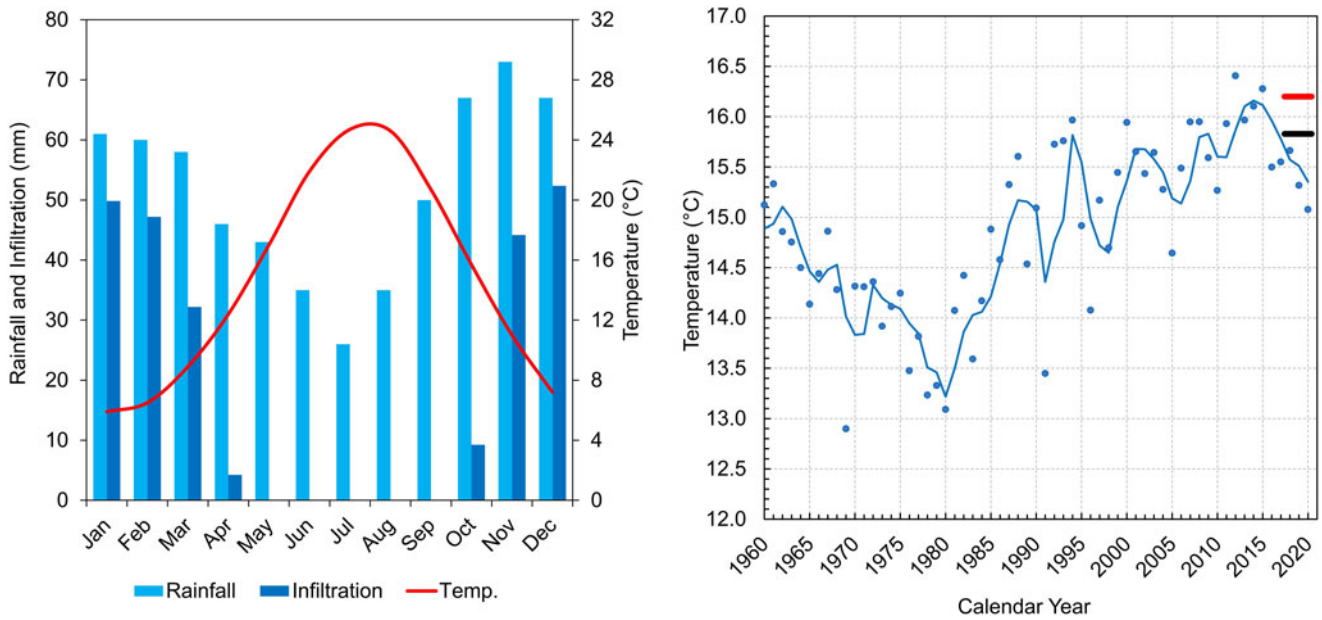
Figure 3. Left panel: mean monthly rainfall, infiltration, and temperature at Altamura for the period 1960–2020. Right panel: mean annual temperatures at Altamura 1960–2020. The blue line represents the 3-year running mean, while the red and the black horizontal lines indicate the mean annual temperature between August 2017 and August 2020 in Lamalunga Cave towards the South End (red) and in the Abside chamber (black).

and ε is the initial phase of the signal (Carslaw and Jaeger, 1959). Following the approach of Smerdon et al. (2003) and Domínguez-Villar et al. (2013, 2023), we calculated the wave vector k from the slopes of the linear regressions between the rock thickness (depth z), the natural logarithm of the thermal amplitude ω, and the phase shift ε of the annual signal (Fig. 5a, b):

$$\text{Phase shift (rad)} = 0.176z + 0.507 \rightarrow (R^2 = 0.994) \quad (4)$$

$$\text{Ln } (T_a)(^{\circ}C) = 0.183z + 1.673 \rightarrow (R^2 = 0.995) \quad (5)$$

The solution of equation (3) represents a thermal wave with wave vector $k = (\pi/P\kappa)^{1/2}$, where P and κ are the period of oscillation and the thermal diffusivity of the material, respectively. This formula allows the calculation of thermal diffusivity κ by using the regression slope of both datasets and the corresponding wave velocity $v = (4\pi\kappa/P)^{1/2}$ (Table 2).

The calculated mean wave vector $k = 0.178 \pm 0.01$/m, the thermal diffusivity $\kappa = 30.8 \pm 2.3 \times 10^{-7}$ m^2/s and the wave velocity $v = 34.2 \pm 1.3$ m/yr are much higher that the values calculated in soil profiles where the heat transmission is dominated by conduction and characterized by k values around 0.5 (Fig. 5). Less-steep slopes ($k = 0.4$–0.3) can indicate air-filled cavities and passages in the host rock and/or the contribution of thermal convection, while the slope approaches 0 for tunnel caves and highly ventilated passages dominated by convective airflow (Smerdon et al., 2003; Badino, 2010; Domínguez-Villar 2013). For sites influenced only by thermal conduction the wave vector k is mostly related to the thermal diffusion coefficient of the rock/soil cover above the ceiling of the cave and, therefore, is typical for each bedrock/soil cluster as a function of their lithology, porosity, and water content. On the other hand, where thermal convection is also operating, the wave vector k as well as the thermal diffusivity integrate also the contribution of the air flow.

In shallow limestone caves with negligible ventilation, dominated by thermal conduction, thermal diffusivity has been quantified as 7.6×10^{-7} m^2/s (Domínguez-Villar et al., 2013), 8.0×10^{-7} m^2/s (Guerrier et al., 2019) and 5.1×10^{-7} m^2/s (Domínguez-Villar et al., 2023). These values fall within the range of carbonate rocks ranging from $3.1 \times 7.6 \times 10^{-7}$ m^2/s to $15.3 \times 7.6 \times 10^{-7}$ m^2/s (Cermak et al., 1982). In a recent study, Domínguez-Villar et al. (2023) explained the low thermal diffusivity at Los Pilones Cave, Spain ($5.1 \times 7.6 \times 10^{-7}$ m^2/s) as a consequence of the high water content of the host rock related to its enhance porosity (thermal diffusivity of water = $1.4 \times 7.6 \times 10^{-7}$ m^2/s), while higher thermal diffusivity would be associated with air-filled porosity (dry climate settings) given that the κ value of air at standard temperature and pressure is $\sim 186 \times 10^{-7}$ m^2/s (Massman, 1999).

The thermal diffusivity calculated for Lamalunga Cave (κ = 30.8 ± 2.3 10^{-7} m^2/s) is well above the documented range for caves dominated by thermal conduction as well as for carbonate rocks. The reason for the anomalously high thermal diffusivity may be associated with cavity and air-filled porosity in the limestone above the ceiling, as well as derived by the minor contribution of thermal advection in the cave galleries. In this case, the thermal diffusivity should not be referred to the encasing limestone but to the whole rock–air ensemble.

However, the calculation of thermal diffusivity assumes a semi-infinite space as a boundary condition, and if this condition is not satisfied, the thermal diffusivity cannot be calculated by this method. For example, Smerdon and Stieglitz (2006) explored the heat transport of harmonic temperature signals in Earth's shallow subsurface, which highlighted that the temperature oscillations are much less attenuated with respect to the infinite half space scenario in the presence of a lower boundary. In the case of Lamalunga Cave, the lower boundary can be related to the presence of unexplored large deeper galleries connected through fissures to the cave, although no evidence for this currently exists. On the other
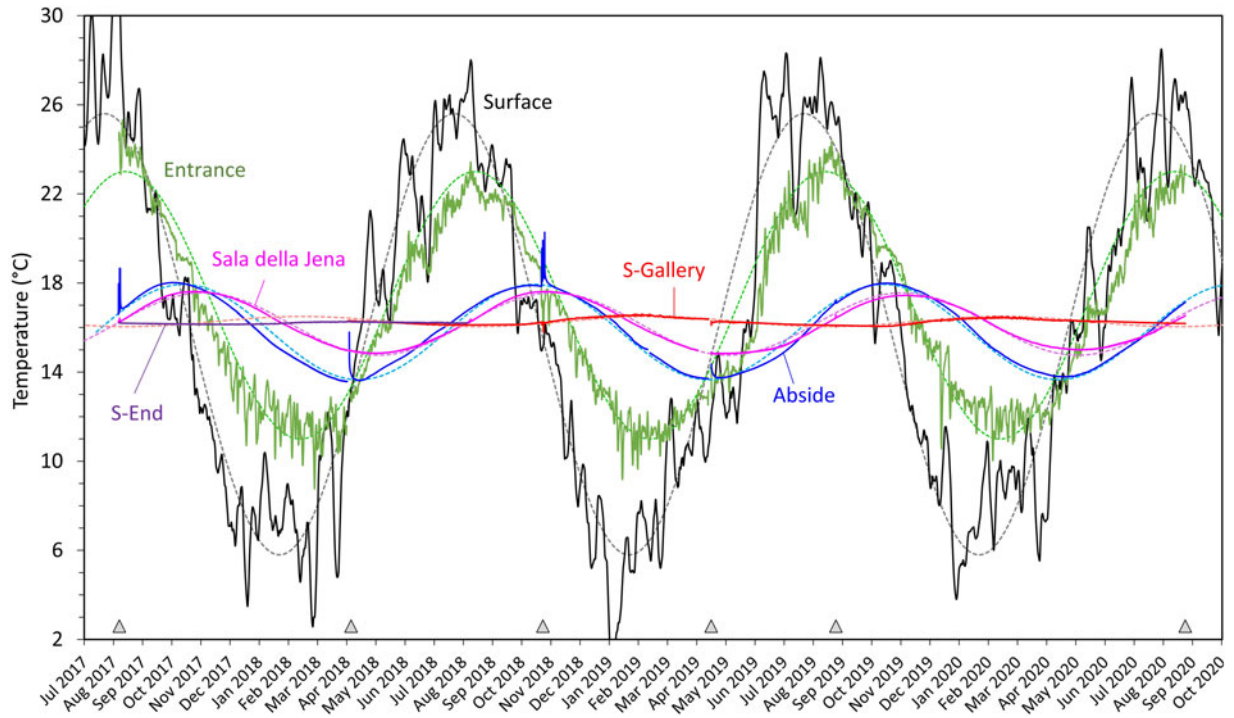
Figure 4. Three-year record of air temperature at five locations in Lamalunga Cave compared to the surface air temperature record (Altamura station). The dashed lines indicate the modeled temperatures calculated with sinusoidal functions (see text). The record for the South End (S-End) is limited to the first year due to data logger malfunction. The triangles mark the visits inside the cave that lasted about 6 hours/day for periods between one and four days. The sudden cave temperature anomalies in August 2017, April 2018, October 2018, and April 2019 are related to visits to the cave.

hand, the influence of a phreatic level close to the cave can be ruled out because the phreatic level in this part of the High Murge plateau is more than 200 m below the surface (Parise, 2011).

Whatever the reason, Lamalunga Cave exhibits a reduced attenuation of the seasonal signal with respect to other published cave sites, which allows detection of annual temperature cycles as deep as 25 m below the surface.

The influence of water infiltration

When comparing MAT between cave sites and surface, it is noteworthy that all cave MATs are significantly higher than the surface MAT. This is particularly true for the South Gallery, where MAT is 0.7°C higher with respect to the surface MAT recorded during the same period. This result should be expected because the hill slope under which the cave developed lacks arboreal vegetation cover and is facing SE, thus receiving a significantly higher
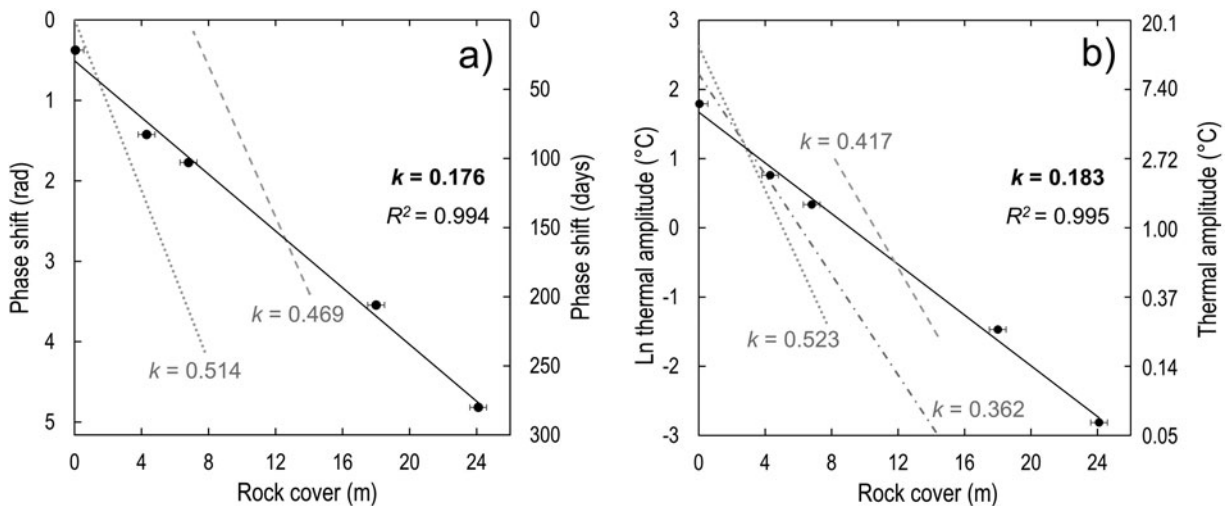

Figure 5. Correlation between rock cover and phase shifts (a) and between rock cover and thermal amplitude (b) for the cave temperature time-series with the corresponding *k* values. The slope of the regression line is compared with the slopes calculated from a shallow cave in central Spain (gray dash–dot line: Domínguez-Villar et al., 2013), the entrance narrow gallery of Los Pilones Cave, Spain (gray dashed line: Domínguez-Villar et al., 2023), and in a soil profile in North Dakota, USA (gray dotted line: Smerdon et al., 2003) (see text).

Table 1. Statistics of Lamalunga Cave temperature measurements and corresponding modeling parameters of the sinusoidal functions for the period 2017–2020.

					Modeling parameters	
Point	Rock cover[1] (m)	Distance from entrance[2] (m)	Mean annual Temperature (°C)	SD Temp. Residuals[3] (°C)	Thermal amplitude (±°C)	Phase shift[4] (days)
Surface			15.53 ± 7.70	n.d.	4.95	0
Entrance	0.05[5]	2	16.50 ± 4.05	± 0.5228	3.00	22
Abside	4.3	53	15.83 ± 1.50	± 0.0021	1.07	83
Sala della Jena	6.8	28	16.17 ± 0.95	± 0.0035	0.7	103
South Gallery	18.0	48	16.27 ± 0.14	± 0.0054	0.11	206
South End[6]	24.1	97	16.20 ± 0.04	± 0.0037	0.03	280
Main gallery[7]			16.21 ± 0.48			
Water main gallery[7]			14.84 ± 0.41			

[1]Rock cover includes bedrock and soil (where present).
[2]Distance from entrance includes the vertical distance along the Entrance pit.
[3]Standard deviations (SD) of temperature residuals are calculated with respect to the running 24-h average values.
[4]Phase shifts are calculated with respect to the date of the maximum temperature at the surface.
[5]Rock cover above the measuring point along the entrance pit was arbitrarily set at 0.05 m as representative of the thermal characteristics of the double-steel trapdoor.
[6]Temperature measurements in the South End lasted from August 2017 to July 2018.
[7]Average value of Sala della Jena, South Gallery, and South End series.

amount of solar radiation (Domínguez-Villar et al., 2013). On the other hand, the Abside chamber displays systematically lower (−0.4°C) MAT with respect to the South Gallery. The lower MAT in the Abside, with respect to any other measured point on the cave, likely is related to the fact that most infiltration is concentrated in the Abside chamber and, to a minor extent, in the northern galleries, whereas infiltration in the South Gallery is very limited. Given that the infiltration occurs almost exclusively during the winter months (November–March), it produces a "forced cooling" in the galleries where it occurs. Differential heating (or cooling) in the cave MAT with respect to the surface MAT of up to 3°C has been documented in areas where the infiltration is concentrated during the summer or winter months (Badino, 2010). This is confirmed by Lamalunga Cave dripwater temperature measurements (average 14.84 ± 0.41°C), which are systematically lower with respect to the average air temperature (16.21 ± 0.48°C) along the cave main gallery (Table 1).

Cave ventilation, relative humidity, and CO$_2$ concentration

A few series of spot measurements were performed at 11 points along the main axis of the cave in order to verify the temperature-logger readings and to characterize the seasonal variability of microclimate parameters (temperature, relative humidity, and air pCO$_2$).

Table 2. Wave vector, thermal diffusivity, and wave velocity calculated from the linear regression of the natural logarithm of the thermal amplitude and the from phase shift as a function of the thickness of rock/soil cover.

Regression method	Wave vector k/m	Thermal diffusivity κ (m^2/s)	Wave velocity v (m/yr)
Ln Thermal amplitude	0.183 ± 0.01	29.6 ± 2.2×10^{-7}	34.2 ± 1.3
Phase shift	0.176 ± 0.01	32.0 ± 2.5×10^{-7}	35.5 ± 1.4
Average	**0.180 ± 0.01**	**30.8 ± 2.3×10^{-7}**	**34.2 ± 1.3**

By considering a temperature phase shift of around three months in the northern part of the cave (which exhibits greater seasonal temperature fluctuations), the expected warmer period should occur in October–November, while the cooler period should be in April–May (Fig. 4, Table 2). These shifts are reflected in the temperature profiles. In fact, by excluding the clear perturbation in the area near the base of the entrance pit, a nearly exponential decrease from the homothermic South Gallery towards the Abside chamber in April can be observed, and a corresponding nearly exponential increase occurs in October (Fig. 6). By contrast, quasi-homothermic conditions characterize the entire cave in late January and late July (Figs. 4, 6). The relative humidity profiles follow the surface seasons because they are influenced by rainfall and evapotranspiration, with minimum values in August and near-saturated conditions in winter and spring.

Only four series of air pCO$_2$ could be performed along the axial part of the cave (Fig. 6b). The CO$_2$ concentrations are relatively stable in the South Gallery with values around 8000 ppmv in April 2018 and 4000 ppmv in August 2017. CO$_2$ concentrations tend to gradually increase/decrease in the northern part of the cave.

Cave entrance opening and transient phenomena

The opening of the trapdoor at the cave entrance affects all the microclimate variables and is particularly evident when the atmospheric pressure at the surface is high or increasing rapidly. In order to assess its effect, and the microclimate perturbations related to the presence of visitors inside the cave, we monitored the temperature fluctuations with respect to cave CO$_2$ concentration, relative humidity in the entrance pit, and the atmospheric surface air pressure (SAP).

During the visits on 23–26 October 2018 the surface temperature was slightly lower than the cave temperature, which caused short-lived negative temperature peaks along the South Gallery during the inflow events of 23 October 2018 and 25 October 2018 (Fig. 7) when the SAP was high or rising. On the other hand, on 24 October 2018 and 26 October 2018 the atmospheric
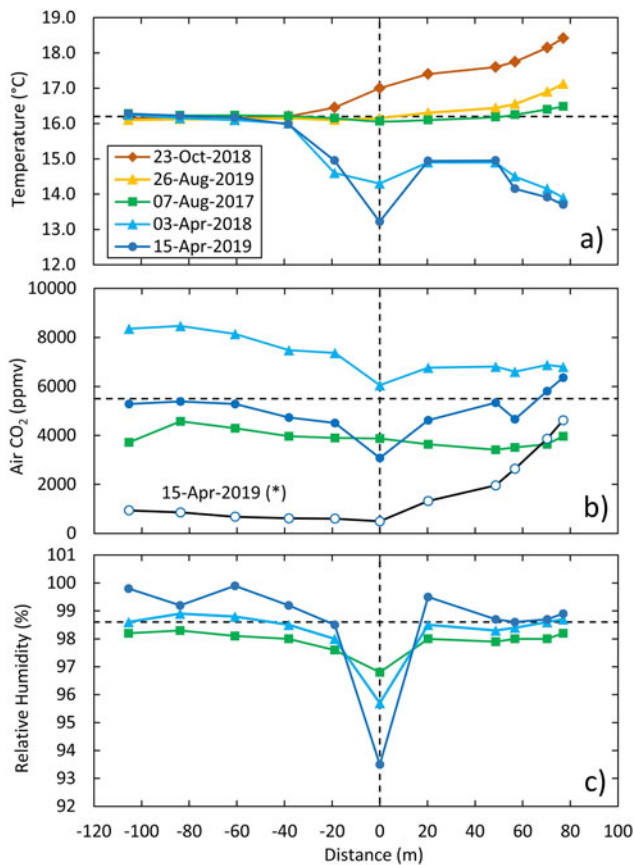
Figure 6. (a) Temperature, (b) CO_2, and (c) relative humidity profiles in different months along the main axis of the cave (see Fig. 1). The distances are calculated from the Entrance Hall towards the Abside chamber at the NE end of the cave. The dashed horizontal lines on the graphs represent the mean annual values for the inner parts of the cave. In (b) the black line represents the concentration profile on 15 April 2019 measured approximately three hours after the opening of the entrance trapdoor in correspondence with a rapid rise in the surface air pressure (see text).

pressure was low and/or lowering, and the air current was reversed with flux estimated around 1 m³/s in the key-hole passage at the base of the entrance pit exiting the cave, which caused a modest negative peak in the entrance pit temperature. During four October visits, two persons were present most of the time in the Abside chamber, which caused transient temperature rises of up to 2°C, although the air temperature inside the Abside chamber switched back to pre-event values in 24 hours.

In the period 7–9 August 2017 the rising atmospheric pressure during the first two visits (7 and 8 August 2017) triggered the sucking of warm air inside the cave (Fig. 8), with a steady air inflow detected in the key-hole passage at the base of the entrance pit with estimated fluxes around 1 m³/s. This caused a slight air temperature rise in the areas near the base of the entrance pit (Entrance Hall and Sala Jena), whereas no appreciable temperature change was detected in the deeper part of the cave (South End). The 07 August 2017 event lasted only 1 hour and resulted in a short negative peak in the CO_2 concentration, whereas on 08 August 2017 the sudden atmospheric pressure rise triggered an inflow event lasting around 3 hours that resulted in a dramatic fall in the CO_2 concentration from 4500 to less than 1000 ppmv in the Entrance Hall. On the other hand, on 09 August 2017 the atmospheric pressure was high but lowering, which caused only a short-lived inflow event with a negligible negative

peak in the CO_2 concentration that was swiftly canceled by the reversing air flow (Fig. 8). In all the three visits, the cave CO_2 concentration and temperature switched back to the pre-event values in 4–6 hours as soon as the trapdoor was closed.

A similar situation occurred on the visit of 15 April 2019, which was caused by a steady rise in the SAP (0.5 mbar/hour) that triggered a fast, cold air inflow from the entrance pit with estimated flux around 1 m³/s that lasted about two hours. This resulted in a rapid decrease in the CO_2 concentration in the entire South Gallery from 5040 ± 390 ppmv to 740 ± 150 ppmv and from 5300 to 1900 ppmv in Sala della Jena (Fig. 6).

Ventilation is usually assessed in caves by using Radon-222 (Kowalczk and Froelich, 2010), as well as by studying transient CO_2 episodes (Faimon et al., 2012; Kukuljan et al., 2021; Sainz et al., 2022). If the seasonal CO_2 budget has to take into account the CO_2 outgassing from dripwater entering the cave, as well as other potential in-cave sources (Buecher, 1999; Mattey et al., 2016), these latter are not relevant during rapid ventilation episodes in which surface air with atmospheric CO_2 concentration is forced inside the cave. Of particular interest is the study of d'Aven d'Orgnac (Southern France), a barometric-descending cave with a vertical development similar to Lamalunga Cave, where continuous monitoring of temperature, relative humidity, Radon-222, and CO_2 concentration allowed the detection of "emptying events" during autumn and winter (Bourges et al., 2001, 2006). These events are triggered by significant SAP variations and cause the almost instantaneous (less than few hours) decrease in cave air temperature, relative humidity, Radon-222, and CO_2 concentration. The subsequent filling periods, during which the pre-event conditions are restored, last about one week. Similar emptying–recharging events in Radon-222 and CO_2 concentration have been described in the Polychrome Room of Altamira Cave (northern Spain), although in this case the events lasting one to more than seven days are symmetrical and triggered by temperature gradients between the surface and the cave air (Sainz et al., 2022).

By applying a simple mass-balance model for the 15 April 2019 event, we can observe that the estimated air inflow for 2 hours (~7000 m³) exceeded the mapped volume of the entire cave. The fast and drastic drop in CO_2 concentration, especially in the South Gallery (volume estimate 4400 m³), which accounts for most of the mapped cave volume, is not compatible with a mixing model. Therefore, other air passages acting as air outflows have to exist, albeit the presence of any other sizable entrances to the cave can be excluded because no entrances are visible in the the barren karst landscape above the cave (Fig. 1b). However, the sporadic discovery in the northern galleries of coprolites of small mammals seems to suggest the existence of cm-wide passages connecting the surface, while the asymmetric lowering of the CO_2 concentration between the South and the northern galleries suggests that forced outflow from the cave preferentially occurs in the South Gallery. This situation is similar to that of Obir Cave (Austria) and Aven d'Orgnac where ventilation occurs through karst micro- and macrofissures and a network of inaccessible (or unexplored) underground passages (Spötl et al., 2005; Bourges et al., 2006).

Daily to sub-daily temperature cycles

Perturbations and daily to sub-daily cycles in the cave microclimate parameters are well known in the literature, and can affect air temperature, relative humidity, dripwater flow rate,
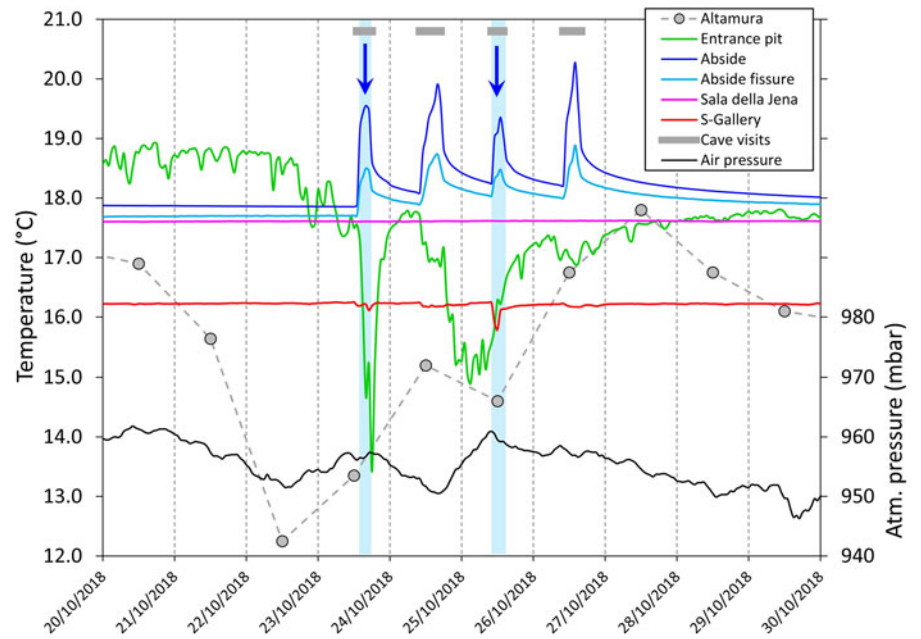
Figure 7. Temperature fluctuations during the four visits to the cave 24–27 October 2018 compared to the external air pressure and mean daily temperature from the Altamura station. During each visit, the duration of which is indicated by gray bars at the top of the graph, the trapdoor at the entrance remained open, thus enhancing the cave ventilation. The pale blue vertical bars and the blue arrows indicate the sucking of cold air inside the cave.
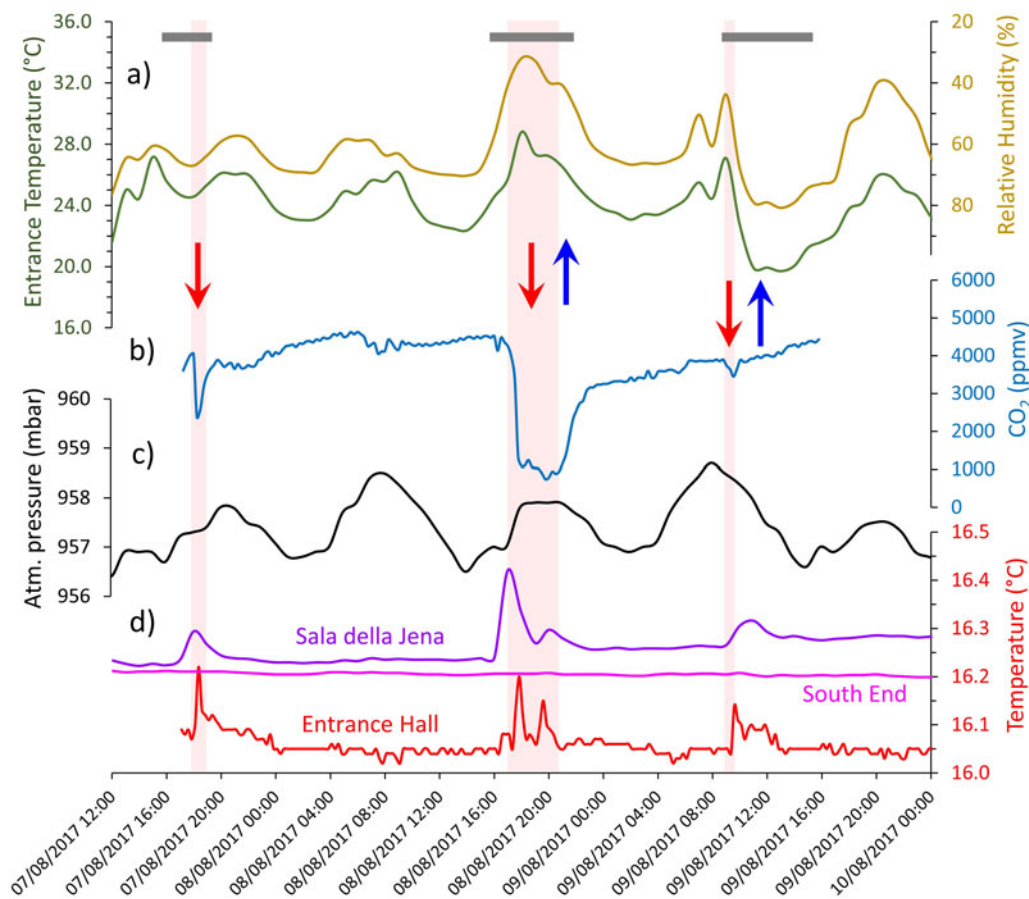

Figure 8. Microclimate regime during the visits to the cave in August 2017. (a) Temperature and relative humidity (reverse scale) fluctuations in the entrance pit; (b) CO_2 concentration fluctuations in the Entrance Hall; (c) variations in atmospheric pressure at Altamura station (hourly values); (d) temperature fluctuations in the Entrance Hall and Sala della Jena. During each visit, the duration of which is indicated by three gray bars at the top of the graph, the trapdoor at the entrance remained open. The pink vertical bars and the red arrows indicate the sucking of warm and low-CO_2 air inside the cave, whereas the blue arrows indicate the outflow of cold air, as detected in the key-hole passage at the base of the entrance pit. Note that the temperature peaks in Sala Jena were also enhanced by the presence of visitors.

radon-222, CO_2 concentration, and barometric air pressure (Genty and Deflandre, 1998; Perrier et al., 2001, 2004, 2023; Sondag et al., 2003; Bourges et al., 2006; Richon et al., 2009; Drăgușin et al., 2018; Sekhon et al., 2021; Gomell and Pflitsch, 2022). In underground environments and, particularly, in barometric caves, daily to sub-daily cycles are induced by atmospheric pressure variations (APV), which are characterized by strong 24-hour (S1 = 1.0 cpd) and 12-hour (S2 = 2.0 cpd) solar harmonic frequencies (Perrier et al., 2001; Sondag et al., 2003; Richon et al., 2009; Mentes, 2018). Although APV can cause thermodynamic adiabatic thermal changes in the air that exceed 0.1°C/hPa, the thermal amplitude is damped by heat inertia of the rock walls and can be significantly modified by water phase changes in near-saturated conditions (Bourges et al., 2006; Perrier et al., 2023). APV can induce barometric tides S1 and S2 not only in the cave atmospheric pressure and air temperature, but even in cave rock temperatures, although with amplitudes 10 times smaller than for cave air temperature (Perrier at al., 2023). Pressure-induced temperature (PIT) variations are particularly relevant near the cave entrances, producing temperature variations up to 1°C/mBar, while in more-confined galleries the PIT transfer function decreases to few 0.001°C/hPa and increases with the distance to the closest cave wall (Perrier et al., 2001, 2010, 2023).

In their recent study of four barometric caves in France, Perrier et al. (2023) calculated that the modulus, at barometric tide S2, varies from 0.002–0.014°C/hPa, with a median value of 0.0048°C/hPa. In particular, along the Red Corridor of Pech Merle Cave, a dead-end horizontal gallery with a topographic trend similar to that of Lamalunga Cave South Gallery, the PIT modulus at barometric tide S2 is relatively constant throughout the year (~0.0036 ± 0.0007°C/hPa) (Perrier et al., 2023). These small semi-diurnal temperature cycles have been explained by PIT changes that diminished in less than one hour as a result of thermal exchanges with the surrounding rock walls (Bourges et al., 2006). Propagation of the APV underground can be delayed and dampened as a function of the distance from the entrance, the morphology of the entrance, and the topographic trend of the galleries. In their study of Wind Cave and Jewel Cave in South Dakota, Gomell et al. (2022) calculated delays between 38 minutes and 2 hours 22 minutes for distances between 0.4 km and 1.5 km from the entrance.

The time-series of Lamalunga temperature residuals (calculated as differences between the hourly measurements and the 24-hour means) reveals the occurrence of PIT variations at all the monitored sites (Fig. 9). Apart from the Entrance pit, where large daily temperature variations (± 0.523°C) are mainly due to the barometric thermal advection of surface air, the PIT variations
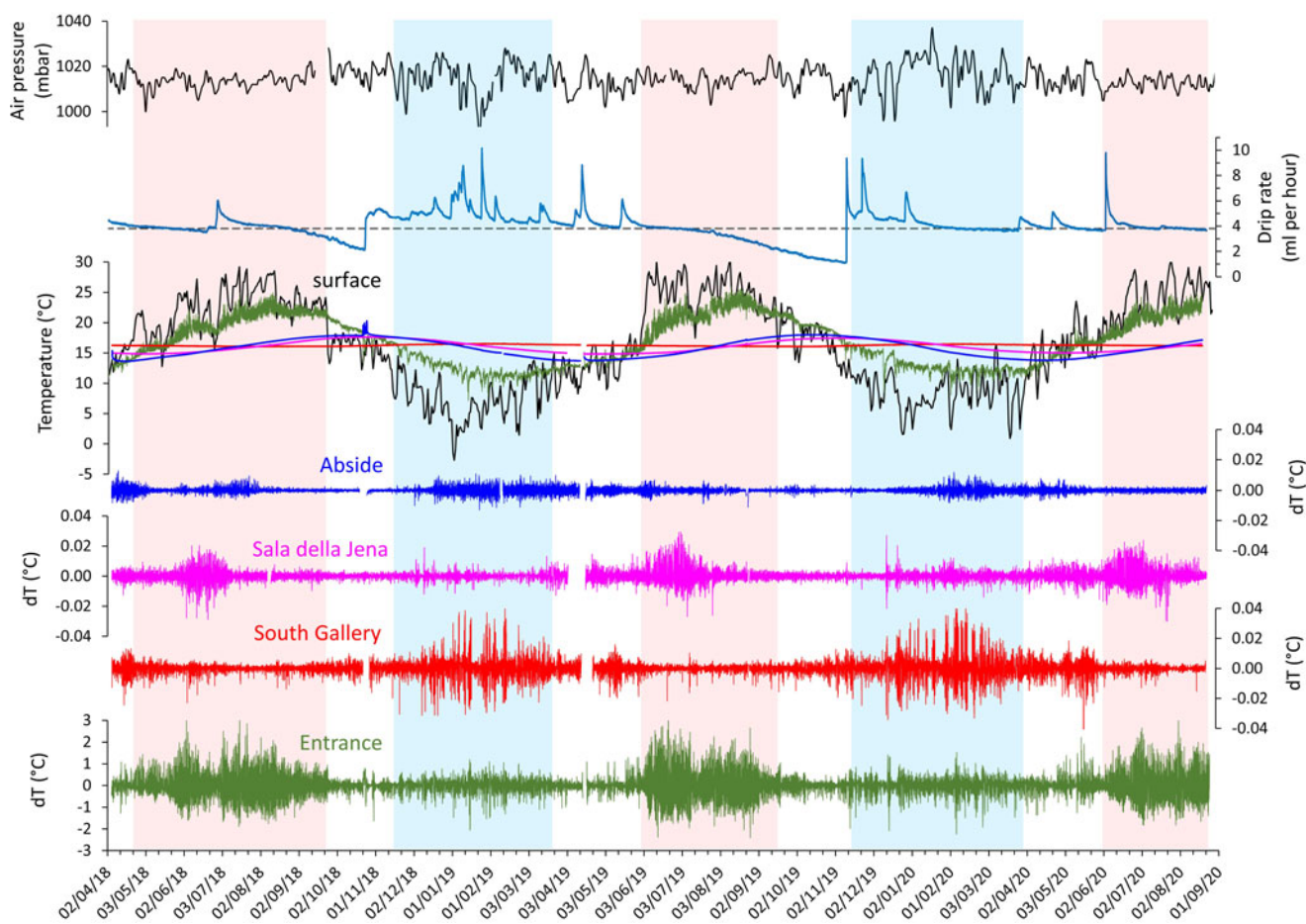

Figure 9. Time-series of surface air temperature and pressure at Altamura station (24-h moving window average) compared to Lamalunga infiltration record, cave temperatures, and their corresponding temperature residuals (dT = differences from the 24-h averages). The pale blue shading indicates winter seasons when the surface temperature was significantly cooler that the cave temperature, while the pink shading indicates summer seasons when the surface temperature was significantly warmer that the cave temperature.
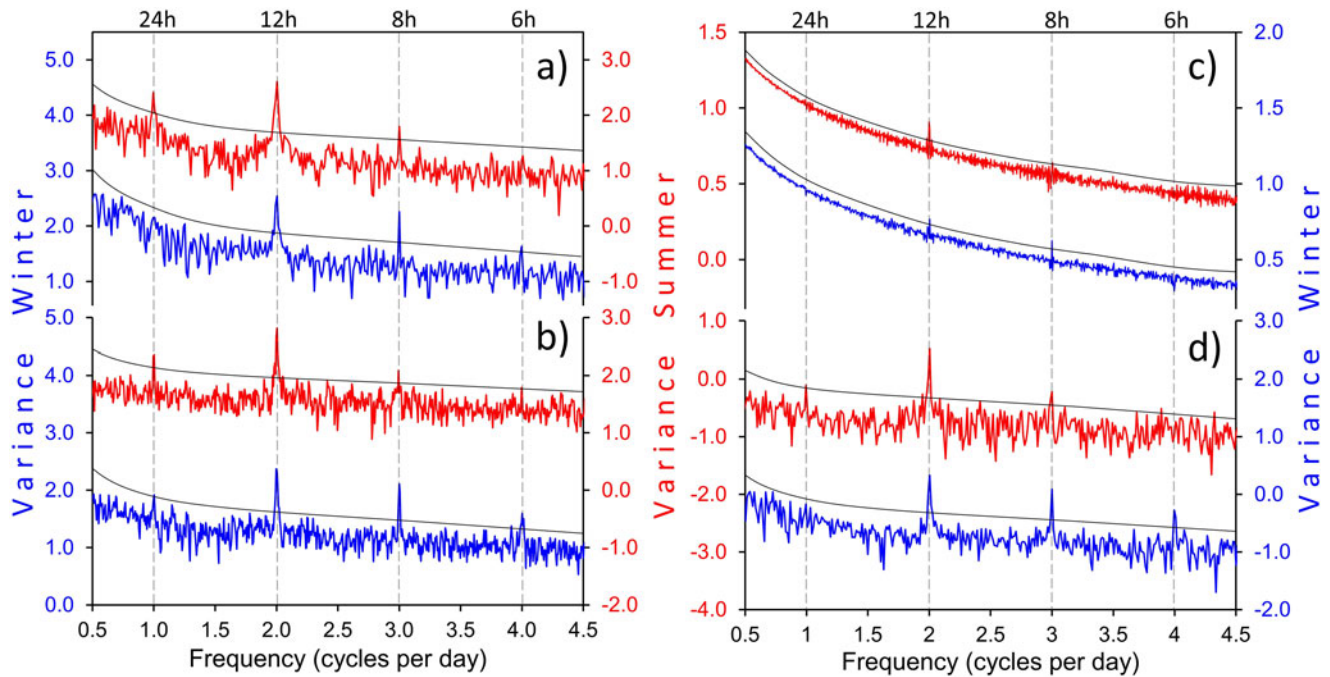
Figure 10. Winter and summer fast Fourier transform for: (a) surface air pressure at Altamura, (b) Lamalunga entrance temperature, (c) Sala della Jena temperature, and (d) South End temperature. Each series is constructed with the data of two consecutive winter (DJF) and summer (JJA) seasons. The black line in each series represents the 90% confidence level.

in the inner cave sites have similar absolute amplitudes with the highest values in the South Gallery (± 0.0054°C), intermediate values in the Sala della Jena (± 0.0035°C) and South End (± 0.0037°C), and the lowest values in the Abside chamber (± 0.0021°C). Although these values are only 1.5–4 times the reported instrumental resolution (0.0014°C), the systematic coherence of the different data loggers and the reproducibility of the signals in three consecutive years corroborate the findings. Moreover, the absolute amplitudes of the PIT variations are remarkably similar to the values observed in other barometric caves in France (Bourges et al., 2006; Perrier et al., 2023). Each site, however, is characterized by a different pattern and seasonality: the Abside chamber and the South Gallery display the highest daily thermal fluctuations in the winter season (December–May) when most of the water infiltration occurs, while Sala della Jena displays higher amplitude in the summer season (June–September), which is similarly to the pattern at the Entrance pit (Fig. 9). Conversely, the South End (not shown) exhibits almost constant daily thermal fluctuations throughout the year.

Spectral analysis
In barometric caves the spectral analysis of temperature time-series can be compared with the corresponding SAP time-series and gives precious information about the thermal confinement of the galleries (Perrier at al., 2023). In order to account for different seasonal behavior, we performed fast Fourier transform (FFT) analysis on series constructed with the data of two consecutive winter (DJF) and summer (JJA) seasons (Fig. 10).

As expected, the results for the Entrance pit are very similar to the SAP, with a clear barometric S1 (24-h) signal, a most prominent S2 (12-h) signal followed by weaker S3 (8-h) and S4 (6-h) harmonic peaks, as already observed in many French caves (Perrier et al., 2023). The presence of a clear S1 peak confirms

that the Entrance pit is thermally influenced by daily temperature cycles, while the lack of S1 peaks in all the cave sites confirms that most parts of the main gallery are thermally confined. Other than the S1 peak, the spectra of the South End are very similar to the spectra of Entrance pit, with S3 and S4 peaks most prominent in the winter season. In the South Gallery (not shown) the FFT spectra are similar to those of the South End, but with only a very weak S2 signal. In contrast, Abside chamber (not shown) and Sala della Jena (Fig. 10c) display a high variance range and very weak S2 signal. This difference possibly is related to the position of the room at the intersection of two galleries, and/or to the periodic water infiltration, with subsequent water films flowing on the rock surface, and to evaporation–condensation episodes.

Seasonal variations, phase shifts, and delays
In order to evaluate seasonal behavior, phase shift, and delays in the daily temperature cycles we used a graphical approach, which is better suited to illustrate the complexity of the mechanisms acting simultaneously in different parts of the cave and during different seasons. For this, we analyzed three time slices: (1) January, when the surface temperature is lower and the cave is almost in homothermic condition; (2) June, when the surface temperature is high but the northern part of the cave (Sala della Jena and Abside) has the lowest temperatures; and (3) September, when the external temperature is still high and temperatures in the northern part of the cave are close to their maximum values (Fig. 4).

Comparison between the surface air pressure residuals (SAPr) and the Entrance pit temperature residuals (TEPr) revealed that the temperature cycles are synchronous (within the range of the acquisition frequency of 1 hour) and mimic, in most details, the SAP variations (Fig. 11a, e, i). The SAP-to-air temperature transfer function varies from 0.5–1.0°C/mBar in summer and from
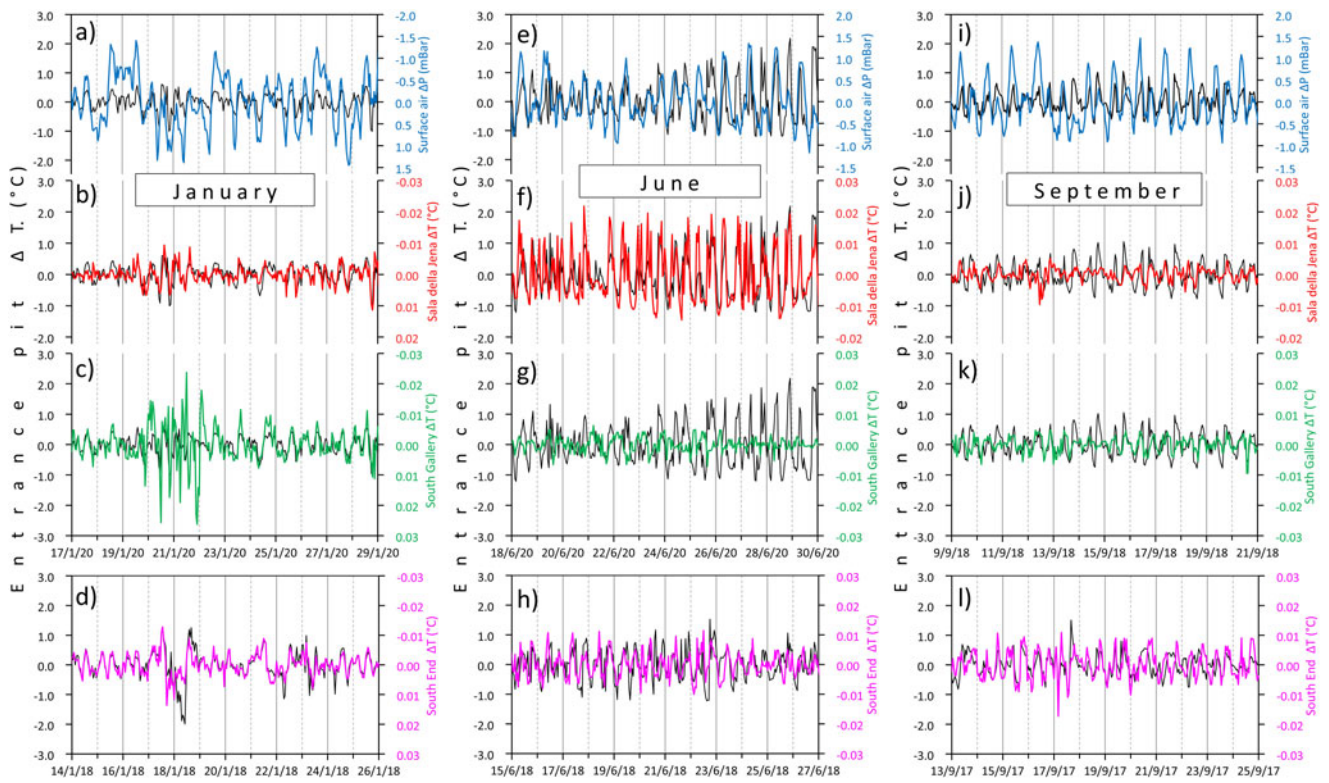
Figure 11. Time-series of surface air pressure (Altamura station) and cave temperature residuals during three significant periods representing (a–d) the winter season (January 2018), (e–h) early summer (June 2018), and (i–l) late summer (September 2017) (see text). Note the inverted scale on the January secondary axes (a–d).

−0.2°C/mBar to −0.32°C/mBar in winter, which confirms that thermal advection is actively operating along the entrance pit. Some details, however, can differ as a result of the distance from the cave of the Altamura meteorological station (6 km). For this reason, we used the Entrance pit TEPr as a proxy for the SAPr at the cave site in order to compare the temperature residuals in the inner part of the cave. This hypothesis was corroborated by the fact that temperature residuals in the internal cave sites systematically have a higher correlation coefficient with TEPr than with SAPr.

Sala della Jena temperature residuals (TJEr) exhibited larger daily fluctuations in summer, especially in June and July (Fig. 9), while for the rest of the year the daily fluctuations were more muted (Fig. 11b, f, j), which is similar to the signal in the TEPr. The SAP-to-air temperature transfer function varies from 0.0013–0.003°C/mBar in summer and from 0.0012–0.0015°C/mBar in winter, suggesting a minor influence of barometric thermal advection especially in summer. The South Gallery temperature residuals (TSGr), on the other hand, exhibit a more complex behavior with the best correlation to TEPr in winter and late summer but no clear correlation in the intermediate seasons (Fig. 11 c, g, k). The South End temperature residuals (TSEr) are correlated more consistently to TEPr throughout the year, regardless of the thermal conditions at the surface (Fig. 11d, h, l), with SAP-to-air temperature transfer function varying from 0.0048–0.0033°C/mBar in summer and from 0.0018–0.0024°C/mBar in winter. Only in the Abside chamber did temperature residuals (not shown here) have no clear cyclicity without a consistent correlation with both SAPr and TEPr.

The information gathered from quantification of the thermal diffusivity, the analyses of the annual temperature cycles, the FFT spectra, and the study of the temperature residuals allow detailed description of barometric air flow inside Lamalunga Cave and the possible contribution of barometric and thermal advection. We summarized the results in two diagrams that represent the winter and summer situations (Fig. 12). In summer, the overpressure created by rising SAP gently pumps warm air inside the cave with strong thermal advection in the Entrance pit and a limited influence up to Sala della Jena, while in the other parts of the cave no measurable thermal advection is detectable, and the daily temperature fluctuations are controlled mainly by PIT variations. The air flux and thermal advection are reversed during under-pressure created by lowering SAP. In January, most of the cave is at near-homothermic condition and the thermal advection is mostly confined to the Entrance pit. However, as towards both cave ends (Sala della Jena and South End) where the SAP-to-air temperature transfer function is systematically higher in summer than in winter, a minimal influence of thermal advection has to operate. Because the relative humidity of surface air is generally much lower than inside the cave, the faint air flow can play a crucial role in the growth and morphology of delicate speleothem formations such as coralloids which grew from hydro-aerosol, evaporation, and capillary flow (Vanghi et al., 2017, 2019).

The absence of thermal perturbation during winter, when cold and dense external air can potentially sink inside the cave, testifies to the limited extent of this phenomenon and the mitigation mechanism produced by the Entrance pit whose narrow diameter hinders temperature transmission inside the main gallery of the
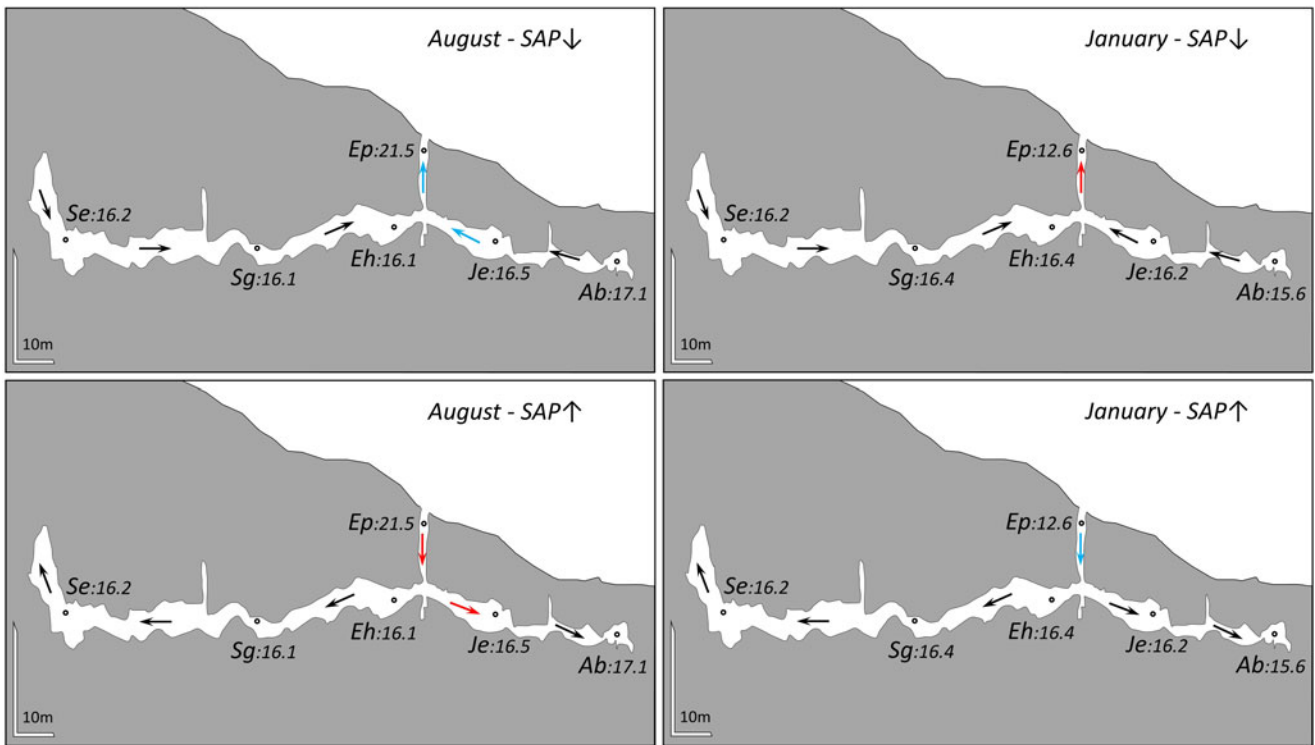
Figure 12. Simplified cross section of Lamalunga Cave (vertical exaggeration = 3) with air-flow direction in summer (August) and winter (January) as a function of surface air pressure rise (↑ = overpressure) and fall (↓ = underpressure). Ep = Entrance pit; Se = South End; SG = South Gallery; Eh = Entrance Hall; Je = Sala della Jena; Ab = Abside. The number near each station is the mean daily temperature recorded in each month. The arrows indicate the direction of air flow inside the cave, with the colors indicating the influence of thermal advection: red = warm; blue = cold; black = no detectable thermal advection (see text).

cave. In this regard, the partial closure of fissures along the trapdoor effectively hinders rapid and dynamic exchange with the surface, although the constriction does not cut off smooth and continuous equilibration with the surface air pressure, thus conveying a tiny convective temperature signal even in the deeper parts of the cave. It has to be noted, however, that the contribution of thermal convection in most parts of the cave is minimal, affecting the thermal regime in the order of magnitude of hundredths of a degree Celsius without adding any significant noise to the temperature records, and this allows the detection of barometric tides throughout the year in all the cave galleries.

Speleothem formation in Lamalunga Cave

Speleothem formation in ventilated galleries depends on a number of variables, which can vary on a seasonal to daily basis and include drip rate, temperature, air CO_2, calcite supersaturation, relative humidity, and the presence of trace elements, impurities, and organic matter (Frisia et al., 2000). High drip rates and low to moderate calcite supersaturation (SI_C) are associated with flowstone and dome-shaped or cone-shaped stalagmites, whereas low drip rates and higher calcite supersaturation favor the formation of candle-shape stalagmites (Miorandi et al., 2010). Conversely, in the absence of direct dripping, minute calcite coralloids can grow from hydro-aerosol generated by the fragmentation of drops (popcorn coralloids; Vanghi et al., 2017) or from evaporation and through intercrystalline and intercorralloid capillary flow (branching coralloids; Caddeo et al., 2015). Both popcorn and branching coralloids are present in Lamalunga Cave

and their distribution is related to the hydrological and microclimate conditions of the different parts of the cave.

Lamalunga Cave water, which was analyzed during 2017 and 2018, revealed substantial spatial and seasonal homogeneity, with low Mg/Ca molar ratio (0.12 ± 0.03) and moderate calcite supersaturation in both drips ($SI_C = 0.45 \pm 0.05$) and pools ($SI_C = 0.44 \pm 0.08$) (Vanghi et al., 2019). This suggests a limited modification of dripwater by prior calcite precipitation, and the potential of calcite precipitation on speleothem surfaces. In these situations, ventilation controls the actual SI_C by lowering the air CO_2 during SAP rises, particularly during the fast emptying events.

Given that infiltration is preferentially concentrated in the northern galleries, a higher density of large popcorn coralloids (Vanghi et al., 2017) is expected in this part of the cave (Fig. 2a, c). The fabric of these coralloids varies from columnar-elongated to fiber-like in their apical parts, alternating with micritic and microsparitic layers that correspond with growth interruptions and condensed intervals (Vanghi et al., 2017). These coralloids are particularly enriched in minor and trace elements and impurities, including Mg, Sr, and Si, organized in cyclic lenticular layers (Vanghi et al, 2019), which testify to the more dynamic microclimate and hydrological regime in the Abside chamber. It also has been noted that coralloids in this part of the cave do not show a preferential orientation of growth, which should have been expected in the presence of strong air currents.

On the other hand, reduced infiltration along the South Gallery explains the absence of large popcorn coralloids and the high density of delicate branching coralloids, which grew from

evaporation and through intercrystalline and inter-coralloid capillary flow (Caddeo et al., 2015; Vanghi et al., 2017) (Fig. 2b, d). These coralloids, made by honey-yellow translucent compact columnar calcite with few impurities and low trace element content, are concentrated preferentially along the edges of limestone debris on the floors of the galleries, often aligned in delicate rows that are spaced several mm apart (Fig. 2b, d). Both globular and dendritic branching morphologies are present, the latter preferentially concentrated on the debris covering the cave floor.

The delicate morphology, low trace-element content, and compact translucent fabric all indicate a very stable environment without significant changes in temperature, relative humidity, and calcite supersaturation (Frisia and Borsato., 2010). This, again, confirms the confined state of the South Gallery where the exceptionally stable temperature, the near-saturation relative humidity favored by steady water infiltration during the winter combined with high air CO_2 concentration prevent any fast coralloid growth, and allow the development of delicate and branching morphologies. Given that most of the coralloid growth occurred in the Holocene and 64–36 ka (Vanghi et al., 2019), their ubiquitous presence in the South Gallery suggests that stable microclimate conditions persisted for several tens of thousands of years inside the cave.

CONCLUSIONS

This study reveals the complex behavior of thermal exchange and ventilation in shallow caves and how the thickness of the rock above the ceiling of the galleries influences microclimate and, eventually, speleothem formation.

The South Gallery, with a rock overburden of more than 20 m, is characterized by reduced water infiltration and almost homothermic conditions, with an annual thermal amplitude around ± 0.15°C. Here, delicate branching corralloids are the most common speleothem morphotype, while active-forming stalagmites are absent. At the other end, the shallower northern galleries are characterized by rapid infiltration events and annual sinusoidal cycles with a thermal amplitude of up to ± 2.1°C. These conditions favor the growth of abundant popcorn corralloids and spray-deposit speleothems. Given the extremely slow growth rate of corralloids (0.2–0.4 mm/ka), their presence and morphology are valuable indicators of the stable hydrological and microclimate conditions inside the cave over tens of thousands of years.

This is the first study that combines the analysis of air temperature annual cycles, spectral analyses of air temperature residuals, and the study of rapid CO_2 events to characterize the ventilation regime inside the cave. As such, it can help understand microclimate dynamics in other shallow caves that eventually influence the morphology and the geochemical properties of speleothems utilized as recorders of past climate changes.

CRediT author statement

AB: Conceptualization, methodology, investigation, data curation and analysis, visualization, writing – original draft preparation. MS: Investigation, data curation, writing – reviewing and editing. VM: Data curation, writing – reviewing and editing. GM: Supervision, funding acquisition, writing – reviewing and editing.

Declaration of competing interest statement

The authors declare that they have no known competing financial interests or personal relationships that could have appeared to influence the work reported in this paper.

REFERENCES

Agostini, S., 2011. Lineamenti geomorfologici della Grotta di Lamalunga. *DiRe in Puglia* **2**, 17–21.

Badino, G., 2010. Underground meteorology—"What's the weather underground?" *Acta Carsologica* **39**. https://doi.org/10.3986/ac.v39i3.74.

Borsato, A., Frisia, S., Miorandi, R., 2015. Carbon dioxide concentration in temperate climate caves and parent soils over an altitudinal gradient and its influence on speleothem growth and fabrics. *Earth Surface Processes and Landforms* **40**, 1158–1170.

Bourges, F., Genthon, P., Genty, D., Lorblanchet, M., Mauduit, E., d'Hulst, D., 2014. Conservation of prehistoric caves and stability of their inner climate: lessons from Chauvet and other French caves. *Science of the Total Environment* **493**, 79–91.

Bourges, F., Genthon, P., Mangin, A., D'Hulst, D., 2006. Microclimates of l'Aven d'Orgnac and other French limestone caves (Chauvet, Esparros, Marsoulas). *International Journal of Climatology* **26**, 1651–1670.

Bourges, F., Mangin, A., d'Hulst, D., 2001. Le gaz carbonique dans la dynamique de l'atmosphère des cavités karstiques: l'exemple de l'Aven d'Orgnac (Ardèche). *Comptes Rendus de l'Académie des Sciences-Series IIA–Earth and Planetary Science* **333**, 685–692.

Breecker, D.O., Payne, A.E., Quade, J., Banner, J.L., Ball, C.E., Meyer, K.W., Cowan, B.D., 2012. The sources and sinks of CO_2 in caves under mixed woodland and grassland vegetation. *Geochimica et Cosmochimica Acta* **96**, 230–246.

Breitenbach, S.F., Lechleitner, F.A., Meyer, H., Diengdoh, G., Mattey, D., Marwan, N., 2015. Cave ventilation and rainfall signals in dripwater in a monsoonal setting—a monitoring study from NE India. *Chemical Geology* **402**, 111–124.

Buecher, R.H., 1999. Microclimate study of Kartchner Caverns, Arizona. *Journal of Cave and Karst Studies* **61**, 108–120.

Caddeo, G.A., Railsback, L.B., De Waele, J., Frau, F., 2015. Stable isotope data as constraints on models for the origin of coralloid and massive speleothems: the interplay of substrate, water supply, degassing, and evaporation. *Sedimentary Geology* **318**, 130–141.

Carslaw, H., Jaeger, J., 1959. *Heat Conduction in Solids*. Oxford University Press, 512 pp.

Cermak, V., Huckenholz, H., Ryback, L., Schmid, R., Schopper, J., Schuch, M., Stoffler, D., Wohlenberg, J., 1982. *The Physical Properties of Rocks, vol. 1, subvol. a*. Numerical Data and Functional Relationships in Science and Technology. Springer-Verlag, Berlin.

Di Vincenzo, F., Churchill, S., Buzi, C., Profico, A., Tafuri, M., Micheli, M., Caramelli, D., Manzi, G., 2019. Distinct among Neanderthals: the scapula of the skeleton from Altamura, Italy. *Quaternary Science Reviews* **217**, 76–88.

Domínguez-Villar, D., Fairchild, I.J., Baker, A., Carrasco, R.M., Pedraza, J., 2013. Reconstruction of cave air temperature based on surface atmosphere

temperature and vegetation changes: implications for speleoclimate records. *Earth and Planetary Science Letters* **369**, 158–168.

Domínguez-Villar, D., Krklec, K., Sierro, F.J., 2023. Thermal conduction in karst terrains dominating cave atmosphere temperatures: quantification of thermal diffusivity. *International Journal of Thermal Sciences* **189**, 108282. https://doi.org/10.1016/j.ijthermalsci.2023.108282.

Drăguşin, V., Tîrlă, L., Cadicheanu, N., Ersek, V., Mirea, I., 2018. Caves as observatories for atmospheric thermal tides: an example from Ascunsă Cave, Romania. *International Journal of Speleology* **47**, 113–117.

Ek, C., Gewelt, M., 1985. Carbon dioxide in cave atmospheres. New results in Belgium and comparison with some other countries. *Earth Surface Processes and Landforms* **10**, 173–187.

Faimon, J., Ličbinska, M., 2010. Carbon dioxide in the soils and adjacent caves of the Moravian Karst. *Acta Carsologica* **39**. https://doi.org/10.3986/ac.v39i3.76.

Faimon, J., Troppová, D., Baldík, V., Novotný, R., 2012. Air circulation and its impact on microclimatic variables in the Císařská Cave (Moravian Karst, Czech Republic). *International Journal of Climatology* **32**, 599–623.

Follieri, M., Giardini, M., Magri, D., Sadori, L., 1998. Palynostratigraphy of the last glacial period in the volcanic region of central Italy. *Quaternary International* **47**, 3–20.

Frisia, S., Borsato, A., 2010. Karst. In: Alonso-Zarza, A.M., Tanner. L.H. (Eds.), *Carbonates in Continental Settings: Facies, Environments, and Processes. Developments in Sedimentology* **61**, 269–318.

Frisia, S., Borsato, A., Fairchild, I.J., McDermott, F., 2000. Calcite fabrics, growth mechanisms, and environments of formation in speleothems from the Italian Alps and southwestern Ireland. *Journal of Sedimentary Research* **70**, 1183–1196.

Frisia, S., Fairchild, I.J., Fohlmeister, J., Miorandi, R., Spötl, C., Borsato, A., 2011. Carbon mass-balance modelling and carbon isotope exchange processes in dynamic caves. *Geochimica et Cosmochimica Acta* **75**, 380–400.

Genty, D., Deflandre, G., 1998. Drip flow variations under a stalactite of the Pere Noel Cave (Belgium). Evidence of seasonal variations and air pressure constraints. *Journal of Hydrology* **211**, 208–232.

Gomell, A.K., Pflitsch, A., 2022. Airflow dynamics in Wind Cave and Jewel Cave: how do barometric caves breathe? *International Journal of Speleology* **51**, 163–179.

Gregorič, A., Vaupotič, J., Šebela, S., 2014. The role of cave ventilation in governing cave air temperature and radon levels (Postojna Cave, Slovenia). *International Journal of Climatology* **34**, 1488–1500.

Guerrier, B., Doumenc, F., Roux, A., Mergui, S., Jeannin, P.-Y., 2019. Climatology in shallow caves with negligible ventilation: heat and mass transfer. *International Journal of Thermal Sciences* **146**, 106066. https://doi.org/10.1016/j.ijthermalsci.2019.106066.

Jeannin, P.-Y., Liedl, R., Sauter, M., 1997. Some concepts about heat transfer in karstic systems. In: Jeannin, P.-Y. (ed.), *Proceedings of the 12th International Congress of Speleology, La Chaux de Fonds, Switzerland, 10–17 August 1997.* Spéléo Projects, Basel, Switzerland, pp. 195–198.

Kowalczk, A.J., Froelich, P.N., 2010. Cave air ventilation and CO_2 outgassing by radon-222 modeling: how fast do caves breathe? *Earth and Planetary Science Letters* **289**, 209–219.

Kukuljan, L., Gabrovšek, F., Covington, M.D., Johnston, V.E., 2021. CO_2 dynamics and heterogeneity in a cave atmosphere: role of ventilation patterns and airflow pathways. *Theoretical and Applied Climatology* **146**, 91–109.

Lari, M., Di Vincenzo, F., Borsato, A., Ghirotto, S., Micheli, M., Balsamo, C., Collina, C., et al., 2015. The Neanderthal in the karst: first dating, morphometric, and paleogenetic data on the fossil skeleton from Altamura (Italy). *Journal of Human Evolution* **82**, 88–94.

Lisiecki, L.E., Raymo, M.E., 2005. A Pliocene–Pleistocene stack of 57 globally distributed benthic δ^{18}O records. *Paleoceanography* **20**, PA1003. https://doi.org/10.1029/2004PA001071.

Luetscher, M., Jeannin, P.-Y., 2004. Temperature distribution in karst systems: the role of air and water fluxes. *Terra Nova* **16**, 344–350.

Massman, W., 1999. Molecular diffusivities of Hg vapor in air, O_2 and N_2 near STP and the kinematic viscosity and thermal diffusivity of air near STP. *Atmospheric Environment* **33**, 453–457.

Mattey, D., Atkinson, T., Barker, J., Fisher, R., Latin, J.-P., Durrell, R., Ainsworth, M., 2016. Carbon dioxide, ground air and carbon cycling in Gibraltar karst. *Geochimica et Cosmochimica Acta* **184**, 88–113.

Mattey, D.P., Fairchild, I.J., Atkinson, T.C., Latin, J.P., Ainsworth, M., Durell, R., 2010. Seasonal microclimate control of calcite fabrics, stable isotopes and trace elements in modern speleothem from St Michaels Cave, Gibraltar. In: Roger-Son, M. (Ed.), Tufas and Speleothems: Unravelling the Microbial and Physical Controls. *Geological Society of London Special Publications* **336**, 323–344.

Mentes, G., 2018. Investigation of the relationship between rock strain and radon concentration in the tidal frequency-range. *Journal of Applied Geophysics* **155**, 232–236.

Miorandi, R., Borsato, A., Frisia, S., Fairchild, I.J., Richter, D.K., 2010. Epikarst hydrology and implications for stalagmite capture of climate changes at Grotta di Ernesto (NE Italy): results from long-term monitoring. *Hydrological Processes* **24**, 3101–3114.

Parise, M., 2011. Surface and subsurface karst geomorphology in the Murge (Apulia, southern Italy). *Acta Carsologica* **40**, 79–93.

Perrier, F., Morat, P., Le Mouël, J.-L., 2001. Pressure induced temperature variations in an underground quarry. *Earth and Planetary Science Letters* **191**, 145–156.

Perrier, F., Richon, P., Crouzeix, C., Morat, P., Le Mouël, J.-L., 2004. Radon-222 signatures of natural ventilation regimes in an underground quarry. *Journal of Environmental Radioactivity* **71**, 17–32.

Perrier, F., Bourges, F., Girault, F., Le Mouël, J.-L., Genty, D., Lartiges, B., Losno, R., Bonnet, S., 2023. Temperature variations in caves induced by atmospheric pressure variations—part 1: transfer functions and their interpretation. *Geosystems and Geoenvironment* **2**, 100145. https://doi.org/10.1016/j.geogeo.2022.100145.

Pesce Delfino, V., Vacca, E., 1993. An archaic human skeleton discovered at Altamura (Bari, Italy). *Rivista di Antropologia* **71**, 249–257.

Prelovšek, M., Šebela, S., Turk, J., 2018. Carbon dioxide in Postojna Cave (Slovenia): spatial distribution, seasonal dynamics and evaluation of plausible sources and sinks. *Environmental Earth Sciences* **77**, 289. https://doi.org/10.1007/s12665-018-7459-6.

Profico, A., Buzi, C., Di Vincenzo, F., Boggioni, M., Borsato, A., Boschian, G., Marchi, D., et al., 2023. Virtual excavation and analysis of the early Neanderthal cranium from Altamura (Italy). *Communications Biology* **6**, 316. https://doi.org/10.1038/s42003-023-04644-1.

Richon, P., Perrier, F., Pili, E., Sabroux, J.-C., 2009. Detectability and significance of 12 hr barometric tide in radon-222 signal, dripwater flow rate, air temperature and carbon dioxide concentration in an underground tunnel. *Geophysical Journal International* **176**, 683–694.

Riechelmann, S., Breitenbach, S.F., Schroeder-Ritzrau, A., Mangini, A., Immenhauser, A., 2019. Ventilation and cave air pCO_2 in the Bunker–Emst cave system (NW Germany): implications for speleothem proxy data. *Journal of Cave and Karst Studies* **81**, 98–102.

Riga, A., Boggioni, M., Papini, A., Buzi, C., Profico, A., Di Vincenzo, F., Marchi, D., Moggi-Cecchi, J., Manzi, G., 2020. In situ observations on the dentition and oral cavity of the Neanderthal skeleton from Altamura (Italy). *PLoS ONE* **15**, e0241713. https://doi.org/10.1371/journal.pone.0241713.

Sainz, C., Fábrega, J., Rábago, D., Celaya, S., Fernandez, A., Fuente, I., Fernandez, E., Quindos, J., Arteche, J.L., Quindos, L., 2022. Use of radon and CO_2 for the identification and analysis of short-term fluctuations in the ventilation of the polychrome room inside the Altamira Cave. *International Journal of Environmental Research and Public Health* **19**, 3662. https://doi.org/10.3390/ijerph19063662.

Sekhon, N., Novello, V.F., Cruz, F.W., Wortham, B.E., Ribeiro, T.G., Breecker, D.O., 2021. Diurnal to seasonal ventilation in Brazilian caves. *Global and Planetary Change* **197**, 103378. https://doi.org/10.1016/j.gloplacha.2020.103378.

Smerdon, J.E., Pollack, H.N., Enz, J.W., Lewis, M.J., 2003. Conduction-dominated heat transport of the annual temperature signal in soil. *Journal of Geophysical Research: Solid Earth* **108**, 2431. https://doi.org/10.1029/2002JB002351.

Smerdon, J.E., Stieglitz, M., 2006. Simulating heat transport of harmonic temperature signals in the Earth's shallow subsurface: lower-boundary

sensitivities. *Geophysical Research Letters* **33**, L14402. https://doi.org/10.1029/2006GL026816.

Sondag, F., van Ruymbeke, M., Soubiès, F., Santos, R., Somerhausen, A., Seidel, A., Boggiani, P., 2003. Monitoring present day climatic conditions in tropical caves using an environmental data acquisition system (EDAS). *Journal of Hydrology* **273**, 103–118.

Spötl, C., Fairchild, I.J., Tooth, A.F., 2005. Cave air control on dripwater geochemistry, Obir Caves (Austria): implications for speleothem deposition in dynamically ventilated caves. *Geochimica et Cosmochima Acta* **69**, 2451–2468.

Treble, P.C., Fairchild, I.J., Griffiths, A., Baker, A., Meredith, K.T., Wood, A., McGuire, E., 2015. Impacts of cave air ventilation and in-cave prior calcite precipitation on Golgotha Cave dripwater chemistry, southwest Australia. *Quaternary Science Reviews* **127**, 61–72.

Tremaine, D.M., Froelich, P.N., 2013. Speleothem trace element signatures: a hydrologic geochemical study of modern cave dripwaters and farmed calcite. *Geochimica et Cosmochimica Acta* **121**, 522–545.

Vanghi, V., Borsato, A., Frisia, S., Howard, D.L., Gloy, G., Hellstrom, J., Bajo, P., 2019. High-resolution synchrotron X-ray fluorescence investigation of calcite coralloid speleothems: elemental incorporation and their potential as environmental archives. *Sedimentology* **66**, 2661–2685. https://doi.org/10.1111/sed.12607

Vanghi, V., Frisia, S., Borsato, A., 2017. Genesis and microstratigraphy of calcite coralloids analysed by high resolution imaging and petrography. *Sedimentary Geology* **359**, 16–28. https://doi.org/10.1016/j.sedgeo.2017.08.001.

Vieten, R., Winter, A., Warken, S.F., Schröder-Ritzrau, A., Miller, T.E., Scholz, D., 2016. Seasonal temperature variations controlling cave ventilation processes in Cueva Larga, Puerto Rico. *International Journal of Speleology* **45**, 259–273.

Warken, S.F., Fohlmeister, J., Schröder-Ritzrau, A., Constantin, S., Spötl, C., Gerdes, A., Esper, J., Frank, N., Arps, J., Terente, M., 2018. Reconstruction of Late Holocene autumn/winter precipitation variability in SW Romania from a high-resolution speleothem trace element record. *Earth and Planetary Science Letters* **499**, 122–133.

Wigley, T., Brown, M., 1969. Geohydrological implications of cave breathing. *5th Internationaler Kongress für Speläologie Stuttgart 1969, vol. 2: Speleogenesis.* Association of German Cave and Karst Researchers, Munich **2**, 23/1–23/7. [in German]

Zezza, F., 2000. *Grotta di Lamalunga: evoluzione e genesi del sistema carsico sotterraneo.* Celebrazioni per il 50° Anniversario della Fondazione del Centro Altamurano Ricerche Speleologiche (1950–2000). Spelaion 2000, 5 Incontro Regionale della Speleologia Pugliese. Parte Terza: Sessione Scientifica. Uniongrafica Corcelli Editrice, Bari, Italy, pp. 61–74.